# Biodegradable Nanofibrous Scaffolds as Smart Delivery Vehicles for Amino Acids

*Silvana Maione,*[1,2] *Maria M. Pérez-Madrigal,*[1,2] *Luis J. del Valle,*[1,2,*] *Angélica Díaz,*[1,2] *Lourdes Franco,*[1] *Carlos Cativiela,*[3] *Jordi Puiggalí*[1,2] *and Carlos Alemán*[1,2,*]

[1] Department of Chemical Engineering, ETSEIB, Universitat Politècnica de Catalunya, Av. Diagonal 647, Barcelona 08028 (Spain)

[2] Center for Research in Nano-Engineering, Universitat Politècnica de Catalunya, Campus Sud, Edifici C', C/Pasqual i Vila s/n, Barcelona 08028 (Spain)

[3] Departamento de Química Orgánica, Instituto de Síntesis Química y Catálisis Homogénea-ISQCH, CSIC-Universidad de Zaragoza, C/ Pedro Cerbuna, 12, 50009 Zaragoza, Spain

[*] Corresponding authors: luis.javier.del.valle@upc.edu and carlos.aleman@upc.edu

## ABSTRACT

The encapsulation of essential and conditional amino acids (AAs), and their correct preservation prior being ingested, are challenging tasks. Non-polar (Ala and Phe), polar (Cys and Asn) and charged (Lys and Asp) AAs have been loaded into biodegradable and non-toxic poly(tetramethylene succinate) (PE44) nanofibers (NFs) using electrospinning. Loading of AAs affects considerably the morphology, topography, thermal properties and wettability of PE44 NFs. Furthermore, although AAs crystallize in a phase separated from the polymeric matrix, the distribution of such crystals changes into PE44 NFs and is depending on their chemical nature. Release assays in enzyme-free solutions with different polarities evidence that very significant amounts of AAs are retained into the NFs after 7 days, whereas assays in a lipase-containing solution (*i.e.* lipase performs essential roles in the digestion) show an almost complete release after a few hours. The low weight loss detected through enzymatic degradation assays suggests that the lipase preferentially attacks the PE44 regions responsible for the retention of AAs into the biphasic system. Hence the higher accessibility of the enzyme to such domains favours the almost immediate release of the biomolecules. Results displayed in this work combined with the biocompatibility, biodegradability and potential use of PE44 NFs as edible non-nutritional elements, suggest that loaded PE44/AA NFs can be used to supply essential and conditional AAs.

## INTRODUCTION

Coded amino acids (AAs) are not only building blocks of proteins but also play a variety of functions.[1] Among the most relevant are their actions to support the metabolism (*e.g.* glutathione is synthesized from its constituent amino acids by the sequential action of γ-glutamylcysteine synthetase[2,3] and Tyr synthesizes thyroid hormones[4]) and their role to protect the cardiovascular system (*e.g.* the body uses Arg to produce nitric oxide,[5,6] which in turn reduces blood pressure by relaxing muscles in blood vessels[7,8]). From a physiological point of view, AAs are typically classified into three groups: (1) Essential AAs, which cannot be synthesized by the body (*i.e.* His, Ile, Leu, Lys, Met, Phe, Thr, Trp and Val); (2) Non-essential AAs, which are produced by the body (*i.e.* Ala, Asn, Asp and Glu); and (3) Conditional AAs, which are non-essential AAs that transform into essential under conditions of illness and/or stress (*i.e.* Arg, Cys, Gln, Tyr, Gly, Pro and Ser). Essential and conditional AAs come from the diet.

When added to the food of humans and animals, peptides and proteins are typically encapsulated to overcome some of the negative attributes observed when these biomolecules are directly furnished in the food matrix (*e.g.* loss of bioactivity, bitter taste and poor stability).[9] Within this context, systems such as liposomes, cyclodextrins and hydrogels result in appropriate encapsulation matrices that facilitate oral delivery.[10-12] Although many studies related with the immobilization of small peptides (with even only five residues) have been reported,[9,13-15] research on the encapsulation of individual AAs is very scarce.[16,17] In fact, this is an extremely complex task because of the small size of these compounds, which undergo uncontrolled release from the carrier matrix almost immediately through simple diffusive processes. From a practical point of view, the correct encapsulation and controlled release of AAs is very relevant in the livestock and fisheries sectors: a safe and nutritionally improved animal and fish feed supply

ensures healthy animals and people. For example, microparticulate diets with crystalline AAs have embedded into bio-organic matrices (*e.g.* alginate, carrageenan and zein microparticles) loose up to 80% of their AAs within the first minute after suspending the particles in water.[16,17] Lipid-based systems (*i.e.* liposomes and lipid spray beads) are fragile, making difficult microparticles preparation.[18,19]

In a different approach, Mezzenga and co-workers[20] claimed that oleoylethanolamide-based lyotropic liquid crystals are promising vehicles for the controlled release of hydrophilic AAs. More recently, Wenke and co-workers loaded D-AAs in polyurethane scaffolds (*i.e.* cylindrical foams of 3 mm diameter × 6.5 mm height), for local delivery.[21] Loaded D-AAs protected the scaffold from contamination, preventing biofilm formation, which may represent a treatment strategy for infections caused by bacteria contamination. However, although numerous studies focus on the drug or peptide loading-release behaviour of nanofibrous scaffolds,[22-24] no attempt to load electrospun fibres with AAs has been made yet. It is worth noting that the nanofibers can be processed with cattle feed, enabling the delivery of the AAs upon ingestion.

The main aim of this work is to study the loading of AAs into biodegradable non-toxic poly(tetramethylene succinate) (PE44) nanofibers (NFs) using the electrospinning technique. Appropriated incorporation of fibre-based formulations to cattle feed may be an attractive way to supply AAs, thus improving their bioavailability through controlled delivery. More specifically, non-polar (Ala and Phe), polar (Cys and Asn) and charged (Lys and Asp) AAs have been loaded at concentrations of 1% and 10% w/w into PE44 NFs. After this, the effect of the AAs on the wettability and the morphological, topographical and thermal properties of PE44 fibres have been investigated, paying specific attention to the chemical nature of the AA in the variation of such properties.

Finally, release and degradation assays in different environments have been performed to ascertain the advantages and limitations of this AA-loading technology.

## METHODS

***Materials.*** PE44 was prepared by bulk thermal polycondensation of 1,4-butanediol and succinic acid (diol/diacid molar ratio of 2.2/1).[25] The synthetic route is summarized in Scheme 1. Chemical characterization, viscosity and molecular masses were reported in our previous study.[26]

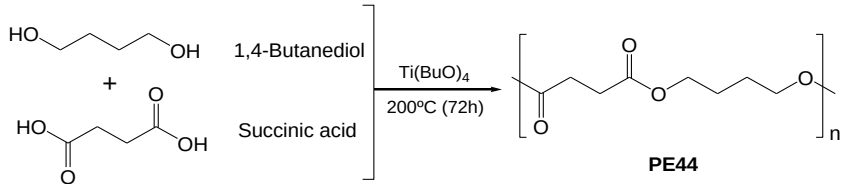


Scheme 1: Synthesis of PE44

L-Alanine (Ala), L-Phenylalanine (Phe), L-Cysteine hydrochloride (Cys), L-Asparagine (Asn), L-Aspartic acid (Asp), and L-Lysine hydrochloride (Lys) were purchase from Sigma-Aldrich. Dichloromethane (ACS reagent, ≥99.5%; each amino acid includes 40-150 ppm amylene as stabilizer), chloroethanol (99% by GC), trifluoroacetic acid (for HPLC, ≥99.0%), and ninhydrin reagent solution were purchased from Sigma-Aldrich. Lipase from *Rhizopus oryzae* (with activity ≥30 U/mg protein) and lipase from porcine pancreas (Type VI-S, ≥20,000 U/mg protein) were purchase from Sigma-Aldrich.

***Electrospinning.*** This method provides a simple and versatile method for generating fibers from a rich variety of materials, including polymers, as has been extensively reported.[27-29] Mixtures of PE44 at concentration 8% w/w and AAs (Ala, Phe, Cys, Asn, Lys or Asp) at concentration 1% or 10% w/w were electrospun. Samples will be named indicating both the AA code and weight percentage (*e.g.* PE44/Ala-10 and PE44/Phe-1

corresponds to a mixture of PE44 with 10% Ala and 1% Phe, respectively). Mixtures were prepared as follows. PE44 was dissolved in a 7:3 dichloromethane : chloroethanol solution, while AAs were dissolved in 200 µL trifluoroacetic acid (TFA). Solutions were kept under stirring for 24 hours at 37 ºC and, finally, they were mixed and loaded in a 5 mL BD plastic syringe for delivery through an 18G × 1.1/2'' needle at a mass-flow rate of 0.5 mL/h using an KDS100 infusion pump. The applied voltage was 20 kV in all cases with exception of Asn-containing mixtures, for which the applied voltage was 15 kV. Thus, for Asn-containing fibres the formation of droplets and electrospun beads was minimized at 15 kV rather than at 20 kV. All electrospun NFs were obtained using a needle tip-collector distance of 18 cm.

***FTIR spectroscopy.*** FTIR spectroscopy was used to assess the composition of the electrospun PE44/AA NFs. Infrared absorption spectra were recorded with a Fourier Transform FTIR 4100 Jasco spectrometer in the 4000-600 $cm^{-1}$ range. A Specac model MKII Golden Gate attenuated total reflection (ATR) with a heated Diamond ATR Top-Plate was used.

***Morphology of electrospun fibres.*** Optical microscopy studies were performed with a Zeiss Axioskop 40 microscope. Micrographs were taken with a Zeiss Axios Cam MRC5 digital camera.

Detailed inspection of texture and morphology of electrospun samples was conducted by scanning electron microscopy using a Focus Ion Beam Zeiss Neon 40 instrument (Carl Zeiss, Germany). Carbon coating was accomplished using a Mitec K950 Sputter Coater fitted with a film thickness monitor *k*150x. Samples were visualized at an accelerating voltage of 5 kV. The diameter of electrospun NFs was measured with the SmartTiff software from Carl Zeiss SMT Ltd using at least 300 values.

***Atomic Force Microscopy (AFM).*** AFM was conducted to obtain topographic and phase images of the surface of NFs using silicon TAP 150-G probes (Budget Sensors, Bulgaria) with a frequency of 150 kHz and a force constant of 5 N/m. Images were obtained with an AFM Dimension microscope using the NanoScope IV controller under ambient conditions in tapping mode. The row scanning frequency was set between 0.4 and 0.6 Hz. The root mean square roughness (Rq), which is the average height deviation taken from the mean data plane, was determined using the statistical application of the NanoScope Analysis software (1.20, Veeco).

***Calorimetry and thermal degradation*** Calorimetric data were obtained by differential scanning calorimetry (DSC) with a TA Instruments Q100 series equipped with a refrigeration cooling system (RCS). Experiments were conducted under a flow of dry nitrogen with a sample weight of approximately 5 mg and temperatures ranges between 20 and 250 ºC. Calibration was performed with indium. Heating runs were carried out at a rate of 20 ºC/min. DSC experiments were performed on PE44 and two representative AA-loaded samples.

Thermogravimetric analyses (TGA) for studying thermal degradation were performed at a heating rate of 20 ºC/min (sample weight *ca.* 5 mg) with a Q50 thermogravimetric analyser of TA Instruments and under a flow of dry nitrogen. Test temperatures ranged from 50 to 600 ºC.

***X-Ray diffraction (XRD).*** The crystallinity of loaded and unloaded NFs was analysed by Wide-Angle X-ray Diffraction (WAXD) using the X'Pert Pro System (PANalytical, Netherland). Diffraction patterns were obtained using Cu Kα (λ= 0.154 nm) X-ray source operating at 30 kV and 30 mA.

***Wettability.*** Contact angle measurements were carried out using the water sessile drop method. Images of milliQ water drops (0.5 μL) were recorded after stabilization

with the equipment OCA 15EC (Data-Physics Instruments GmbH, Filderstadt). SCA20 software was used to analyse the images and determine the contact angle value, which was obtained as the average of at least six independent measures for each sample.

***Release experiments.*** AA-loaded mats were cut into small square pieces (20×20×0.1 $mm^3$) which were weighed (~25 mg) and placed into polypropylene tubes. Phosphate buffered saline (PBS), pH 7.4, and PBS supplemented with 70 *v/v*-% of ethanol (PBS-EtOH) were considered as release media. As PBS-EtOH is more hydrophobic than PBS, comparison of the results in such two environments will provide information about the influence of the hydrophilicity / hydrophobicity of the medium in the release process. More specifically, the addition of ethanol to hydrophilic PBS is expected to cause some swelling effect in the electrospun mats favoring the release of hydrophobic AAs.[30]

Samples (30 mL) were incubated at 37 ºC in an orbital shaker at 80 rpm in tubes of 50 mL. Aliquots of 1 mL were taken at *t*= 0, 0.5, 1, 2, 6, 8, 24, 32, 48, 120, 144 and 168 h for the quantification of released AAs using the ninhydrin reaction, which is described below. After *t*= 168 h, the remaining medium was aspirated quantify the amount of AA remaining in the polymeric matrix. For this purpose, the PE44 matrix was dissolved by placing electrospun samples in eppendorfs with 250 µL of 7:3 dichloromethane : chloroethanol under stirring. Once PE44 was completely dissolved, 1 mL of PBS was added, and the solution was stirred again for 1 hour. Then, solutions were centrifuged and the supernatants (~1 mL) were collected to quantify the amount of AA (see below) that was not released from the electrospun NFs after 168 h. It should be remarked that, in all cases, the sum of AA released along 168 h and the AA remaining at the PE44 matrix corresponded to the amount of AA loaded during the electrospinning process.

Additional release assays were carried out using an enzymatic solution (lipase from *Rhizopus oryzae*) as release medium. PE44/AA-10 samples (*i.e.* mats weighting

approximately 20 mg) were incubated in 1 mL of lipase solution (3.3 mg/mL, $MgCl_2 \cdot 6H_2O$ 0.056% in PBS, pH= 7.2) at 37 ºC and 80 rpm. After *t*= 1, 6 and 24 h, the solutions were centrifuged and the supernatant was removed. The remaining polymeric matrices were washed three times with milliQ water and subsequently dried during 24 h at 37 ºC. After this, matrices were re-dissolved with chloroform (200 µL) to extract the remaining AA. It should be noted that, in this case, the quantification of AAs was performed considering the loaded PE44 matrix rather than the release medium to avoid the interferences induced by the building blocks of the lipase enzyme.

For all release assays, quantification of AAs was carried out using the ninhydrin reaction, which is based on the fact that AAs with a free α-amino group yield a purple (Ala and Asn), blue (Phe and Asp), yellow (Cys) or orange (Lys) coloured product when treated with an excess of ninhydrin. Under appropriate conditions, the colour intensity produced is proportional to the AA concentration. In quantitative estimation of AA using ninhydrin reagent, AA concentration is determined by comparison of the absorbance at 570 nm readings to the standard curve for each AA. Standard curves were performed with stock solutions of AAs prepared at concentrations ranging from 0 to 0.2 mM in milliQ water. Then, 200 µL of nihydrin reagent was added to the stock solution (200 µL). The mixtures were heated at 95 ºC for 15 min and, after this time, they were allowed to cool down at room temperature. Subsequently, the reaction was stopped by adding 300 µL of ethanol (50%) in water. The absorbance was read at 570 nm using aliquots of 30 µL that were previously diluted with 270 µL of milliQ water. The same process was used to determine the concentration of AAs from release assays, 200 µL of AA-containing solution and 200 µL of nihydrin reagent being employed in those cases.

All AA release tests were carried out using three replicates and the results were averaged.

***Hydrolytic, enzymatic and accelerated degradation experiments.*** AA-loaded mats were cut into small square pieces (20×20×0.1 $mm^3$) which were weighed (~25 mg) and placed into polypropylene tubes. The hydrolytic (PBS) and enzymatic (porcine lipase at 1 mg/mL PBS) degradation of AA-loaded mats were studied at 37 ºC. For this purpose, samples placed in a volume of 5 mL were incubated in an orbital shaker at 80 rpm in tubes of 15 mL during four weeks. To prevent microbial degradation, media were supplemented with 0.2 mg/mL sodium azide. In addition, the media were changed to refresh weekly. The accelerated degradation medium consisted of 5 mL of a 1 N NaOH solution and the samples were evaluated at $t$= 30, 60, 90, 120, 150 and 180 min. The weight loss was evaluated using the following expression:

$$Weight\ loss\ (\%) = \frac{W_0 - W_t}{W_0} \qquad (1)$$

where $W_0$ is the dry weight before degradation and $W_t$ is the dry weight at time $t$. All degradation assays were run in triplicate and the results were averaged. The morphology of the samples after degradation was examined by SEM.

## RESULTS AND DISCUSSION

### Preparation and characterization of loaded nanofibers

Figure 1 shows the FTIR spectrum of PE44 and representative PE44/AA-10 NFs in the 1450-1800 $cm^{-1}$ region. The main absorption band, which appears at 1714 $cm^{-1}$, has been assigned to the C=O stretching of the PE44 ester group. Furthermore, a significant band corresponding to $CH_2$ asymmetric and symmetric bending stretching of PE44 is observed at 1470 $cm^{-1}$. The two characteristic bands of AAs and peptides emerge in the 1700-1600 and 1600-1500 $cm^{-1}$ regions in all the spectra of PE44/AA-10 NFs, thus confirming the presence of entrapped AAs in the electrospun mats. Furthermore, the

C=O stretching modes of AAs appear at relatively low wavenumbers (< 1630 $cm^{-1}$) indicating the formation of intermolecular hydrogen bonds, which have been related with the formation of crystals (see below). Unfortunately, the low concentration of AA in PE44/AA-1 NFs precluded their identification in the corresponding FTIR spectra.

Optical micrographs comparing the morphology of unloaded and loaded PE44 NFs are displayed in Figure S1: unloaded PE44 mats consisted in continuous well-defined fibres of homogeneous size, while small beads and heterogeneity appeared after loading AAs. These features were particularly important for the highest AA concentration, as it was corroborated by SEM micrographs (Figure 2). Moreover, AAs caused not only small defects but, in some cases, important morphological changes. For example, the cylindrical shape of PE44 NFs was preserved in matrices loaded with non-polar AAs (Ala and Phe), while a relatively flat ribbon-like morphology was obtained upon the incorporation of Asn and, especially, Cys. In fact, for PE44/Cys samples this effect was detected upon the incorporation of only 1% w/w Cys. These phenomena have been related with the interaction of the AAs with the solvent during the electrospinning process. Thus, velocity of the solvent evaporation, which plays a critical role in fibre formation, is probably affected by AA⋯solvent interactions that in turn depend on the chemical nature of the AA and its affinity by the different solvents participating in the mixture (*i.e.* dichloromethane, chloroethanol and TFA).

Figures S2 and S3 display the diameter distributions of electrospun fibers containing 1% and 10% w/w AAs, respectively, while Table 1 lists the average diameter ($D_{av}$) and the corresponding standard deviation ($\sigma$). The diameter distribution of PE44 fibres is relatively wide with $D_{av} \pm \sigma$ = 386 ± 121 nm. However, the incorporation of AAs not only significantly reduced the fibre diameter (*i.e.* $D_{av}$ ranges from 99 to 140 nm and from 83 to 130 nm for PE44/AA-1 and PE44/AA-10, respectively) but also enhanced in

their uniformity (*i.e.* σ ranges 19 to 31 nm and from 13 to 37 nm for PE44/AA-1 and PE44/AA-10, respectively). The reduction of the fibre diameter has been attributed to the influence of the AAs in the chain entanglement of the solution mixture. Thus, both the incorporation of low-molecular weight AAs and the formation of PE44···AA interactions decreases the degree of chain entanglement in the feeding solution, which is a parameter that significantly influence the fibre diameter.[31]

AFM topography and phase images of the different PE44/AA-1 NFs (Figures 3 and S4), which are consistent with SEM images, suggest that the distribution of the loaded AAs depends on their chemical nature. Thus, PE44/Ala-1 (Figure 3a) and PE44/Phe-1 (Figure S4a) NFs present a smooth surface, no separation between the polymer matrix and the AA being distinguished in corresponding phase images. Accordingly, both Ala and Phe are apparently immobilized inside the polymeric matrix. This is not an unexpected result since electrospun PE44 fibers are very hydrophobic (see discussion of the contact angles below), which facilitate the integration and immobilization of hydrophobic AAs, such as Phe and Ala, through the formation of non-specific van der Waals interactions. In contrast, Lys and Asp are easily observed at the surface of PE44/Lys-1 (Figure 3c) and PE44/Asp-1 (Figure S4c), respectively. Hence, irregular particles of ~30 nm, which have been attributed to crystalized AAs, are embedded at the surface of the NFs following homogeneous distribution. Finally, the characteristics of PE44/Asn-1 (Figure 3b) and PE44/Cys-1 (Figure S4b) are intermediate between those of fibres loaded with hydrophobic and charged AAs. Although Asn- and Cys-containing NFs show particles at the surface, these are significantly smaller and partially immersed into the polymeric matrix. As it was expected, all these trends are more pronounced for PE44/AA-10 NFs. Figure 4 displays the AFM images of PE44/Phe-10 and PE44/Asn-10. The former shows a very smooth surface morphology while the latter exhibits Asn

particles partially immersed in the polymeric phase. Overall, these results reflect that AA···solvent interactions during the electrospinning process are responsible for the distribution of AA particles into the resulting polymeric NFs. Accordingly, non-polar AAs are totally immersed into the polymeric matrix, whereas polar and charged AAs form crystalline domains that remain at the surface of the fibres.

Table 2 presents the root mean square roughness (Rq) of PE44/AA fibres displayed in Figures 3 and 4. The lowest Rq value corresponds to unloaded PE44, increasing for loaded fibres as follows: non-polar AAs (Ala and Phe) < polar AAs (Cys and Asn) < charged AAs (Lys and Asp).

Thermogravimetric analyses (Figure 5 and Table 3) evidenced that all samples are stable up to a temperature 80 ºC higher than the melting point of the PE44 matrix ($T_m$= 112.8 ºC). Incorporation of the AA led to a first degradation step that started at a temperature comprised between 184 ºC and 222 ºC, depending on the AA , which is clearly lower that the initial degradation temperature of PE44 (e.g 299 ºC for 1% weight loss). This first step involved a maximum weight loss of 10%, which is in full agreement with the amount of loaded AA. This step was also detected for the other amino acids although weight loss was lower (i.e. between 3 and 5%). Specifically the maximum temperatures of differential thermal gravimetric analysis (DTGA) curves were between 213-221 ºC range. It should be point out that a continuous degradation was subsequently observed until degradation of PE 44 was predominant.

The degradation behaviour of the PE44/AAs systems differ depending on the loaded AA, as it is deduced from the DTGA curves shown in the inset of Figure 5. Thus, a pronounced degradation step was observed for Cys, Lys and Ala, the maximum temperature of DTGA curves increasing from Cys to Ala. A complex degradation occurs for Phe, whereas Asn and Asp exhibit a continuous weight loss after an initial

process that involved a weight loss lower than 3%. No significant char (*i.e.* less than 0.3%) was observed at temperatures higher than 500 ºC, except for the sample loaded with Lys that rendered a char weight of 3% at 580 ºC.

The second degradation step (*i.e.* that associated with PE44) also depends on the loaded AA: (i) degradation is clearly accelerated with respect to the pure polymer (maximum of DTGA curve at 419 ºC) by the previous decomposition of the cationic form of Lys; (ii) slightly accelerated when Asn or Phe are present; (iii) practically not influenced when Cys and Ala were loaded; and (iv) delayed by the incorporation of Asp, which in fact should correspond to a trifluoroacetate salt.

Thermal properties were analysed by DSC following a three run protocol that consisted on a first heating run (20 ºC/min) of the as-processed samples, a cooling run (10 ºC/min) of previously melted samples after wiping out thermal history for three minutes and finally a third heating run (20 ºC/min) of samples crystallized from the melt. Table 4 summarizes the main data for PE44 and two representatives AA loaded samples, whereas Figure 6 displays the characteristic heating and cooling DSC traces of the studied samples.

The second heating run of PE44 (Figure 6c) exhibits the typical behaviour reported by Yoo *et al.*[32] with an endotherm at 102 ºC prior to the high endotherm at 112 ºC. Double melting peaks have been associated with the fusion of original and thinner crystallites and recrystallized lamellae during the heating process. The total enthalpy is 74.0 J/g, which represents a crystallinity of 67% if the value of 110.3 J/g for a 100% crystalline material is taken into account.[33]

The DSC trace of the initial PE44 scaffold (Figure 6a) shows a single peak at 111.9 ºC, which means that thinner crystals were not thermally stable and underwent the typical reorganization process. Therefore PE44 was able to crystallize during the

electrospinning process but lamellae were less organized that those obtained by crystallization from the melt. In fact, the melting enthalpy sligthly decreases up to 70.8 J/g, which represents a crystallinity of 64%. In contrast, the DSC trace of electrospun samples loaded with AAs exhibit a complex melting peak with a shoulder being clearly identified at 109 ºC and a higher peak at 113-114 ºC that is again associated with reorganized crystals. For these systems, crystallinities are high and close to 65%, which demonstrate the positive effect of the electric field on the molecular orientation. Inset in Figure 6 show also small endothermic peaks at 213.6 and 231.3 ºC (PE44/Phe-10) and 218.6 ºC (PE44/Asn-10), which are related with the previous indicated degradation process of both AAs. In any case, crystals of AAs could not be deduced from DSC data. Nevertheless it should be pointed that the crystallinity of PE44 could increase up to 72% if the AA content is taken into account in the estimation.

Cooling runs (Figure 6b) reveal that AA-loaded samples crystallize with greater difficulty than pure PE44 since exothermic peaks are broader and appear at lower temperatures (*i.e.* 68 and 72.4 ºC with respect to 82 ºC). Crystallization is more difficult for the Phe-loaded sample than for that incorporating Asn, which is less voluminous and more polar. In addition, these DSC traces are highly complex and even show a hot-crystallization peak close to fusion, which shows the difficulty of samples to crystallize during the cooling run. Note also that PE44/Phe-10 presents different endothermic peaks that can be related to phases with different content and also to recrystallization processes. The DSC trace of the PE44/Asn-10 sample illustrates that, after reorganization, thicker crystals with a melting temperature of 113 ºC are formed.

The contact angle values ($\theta$) measured using water (Table S1) indicate that electrospun PE44 matrices are hydrophobic ($\theta$= 129º ± 2º), which should be attributed to both the presence of aliphatic segments and their compact structure within the NFs.

Such hydrophobic character decreases upon the addition of a small amount (1% w/w) of non-polar and polar AAs (*i.e.* $\theta$ comprised between 124º and 110º), whereas incorporation of charged AAs transforms the fibers into very hydrophilic ($\theta$ < 20º). In contrast, all fibres loaded with 10% w/w of AA are more hydrophilic, independently of the chemical nature of the AA. This has been attributed to the increment of the surface roughness caused with the loading (Table 1).

Both 10 % w/w loaded (*i.e.* no clear response was expected from samples loaded with 1% w/w) and unloaded PE44 fibres were characterized by XRD (Figure 7). For unloaded fibres the main peaks correspond to the (020), (021), and (110) reflections, which appear at 2θ= 19.8°, 22°, and 22.6°, respectively (Figure 7a, left).[34,35] Detailed structural analysis was obtained by deconvoluting the XRD spectrum into their three main crystalline peaks and two amorphous halos (Figure 7a, right). The degree of crystallinity ($\chi_c$) of the PE44 matrix was estimated by fitting the XRD profile with the Lorentzian function and, subsequently, applying the following expression:[36]

$$\chi_c = \frac{A_c}{A_c + A_a} \qquad (1)$$

where $A_c$ and $A_a$ are the crystalline and amorphous diffraction areas, respectively, derived from the deconvoluted profiles.

The average crystallite size, $L_{(hkl)}$, in the direction perpendicular to the representative (*hkl*) planes of loaded and unloaded samples was derived from the X-ray diffraction line broadening measurement using the Scherrer equation:[37]

$$L_{hkl} = \frac{0.9\lambda}{\beta \cos\theta} \qquad (2)$$

where λ is the wavelength (CuKα), β is the full width at half maximum height of the (211) line, θ is the diffraction angle and 0.9 is a shape factor. The $L_{(hkl)}$ values for the crystallites perpendicular to the planes (020), (021) and (110) are listed in Table 5.

The degree of crystallinity of unloaded PE44 is $\chi_c$= 0.47 (Table 5), which is consistent with other values reported in the literature.[38,39] For example, PE44 fibres prepared from chloroform : chloroethanol and dichloromethane : dimethylformamide solutions displayed $\chi_c$ values ranging from 0.38 to 0.42[38] and from 0.43 to 0.46,[39] respectively. Therefore, fiber crystallinity decreases with increasing solvent volatility.[40]

The $\chi_c$ values determined for PE44/AA-10 fibers (Table 5) range from 0.55 (PE44/Ala-10) to 0.74 (PE44/Asn-10), thus revealing crystallinities significantly higher than those observed for unloaded fibers. This feature has been associated with the crystallization of AAs among the polymeric chains, as it is proved by comparing the diffractograms recorded for PE44/AA-10 with those of individual crystallized AAs (Figures 7b-7g). Thus, XRD profiles for loaded samples exhibit not only the peaks attributed to the polymeric matrix but also some of the peaks identified for the crystallized AAs (insets in Figures 7b-7g). Overall, XRD and DSC results suggest that AA crystals form initially, subsequently affecting the crystallization and morphology of the polymeric matrix. This observation is supported by changes in the crystallite sizes of loaded samples with respect to the unloaded (Table 5).

**Amino acid release from PE44 fibres**

Quantitative AA release assays were performed with PE44/AA-10 samples (*i.e.* expected uncertainty was too high for assays with 1% w/w AA-loaded fibres) in PBS, PBS-EtOH and an enzymatic environment.

*Release in PBS*. Figure 8a compares the AA accumulated release behavior of all PE44/AA-10 samples when they were exposed to PBS. Release proceeds in a similar way for all samples. Thus, after 1 h an important amount of AA is released to the medium, even though such amount highly depends on the AA. For example, the highest and lowest release after 1 h corresponds to the two polar AAs (78% and 19% for Cys and Asn, respectively). A similar difference was detected for non-polar AAs (57% and 33% for Ala and Phe, respectively) as well as for charged AAs (52% and 33% for Lys and Asp, respectively). After this initial stage, the amount of released AA grows during a few hours for all the systems, even though the stabilization is rapidly reached. The amount of released AA after 168 h comprised between 35% (Phe) and 98% (Cys). Accordingly, Figure 8b which represents the amount of AA retained into the PE44 fibres after 168 h in PBS at 37 ºC, reflecting that the release process cannot be simply related to the polarity of the loaded AA.

*Release in PBS-EtOH*. The AA release profiles in PBS-EtOH for all PE44/AA-10 loaded fibres are displayed in Figure 8c. Amazingly, the more hydrophobic PBS-EtOH environment did not significantly alter the release of Ala and Phe, for which the retention after 168 h increased 11% and 7%, respectively, with respect to PBS (Figure 8b). This feature has been attributed to the fact that these two AAs are immersed into the polymeric matrix. Furthermore, PBS-EtOH also affected the release of Asn, Lys and Asp: the amount of Asn and Asp retained after 168 h increased 20% and 24%, respectively, with respect to PBS, while that of Lys decreased 28%. The only AA that exhibits similar results in PBS and PBS-EtOH is Cys, which experienced an almost complete release after 48 h in both environments. In spite of those differences, the release kinetics of all AAs is similar in PBS and PBS-EtOH, which can be explained by

the Higuchi and first-order models. The Higuchi model, which provides a linear behavior when the cumulative percentage of AA release is represented against the square root of time, indicates that the concentration of AA in the matrix is much higher than the AA solubility, the AA particles (*i.e.* crystals) are smaller than the system thickness, the PE44 swelling and diffusivity are very low and the AA diffusivity is constant. On the other hand, the first order model provides a straight line when the data are plotted as the logarithm of the cumulative percentage of AA release *versus* time, this first order kinetics release reflecting that PE44 can be considered as porous matrix. It is worth noting that the Higuchi and the first-order models are usually combined to describe the first very fast releasing stage and the second very slow releasing stage of the complete profile.[38]

Figure 8 indicates that in many cases the release of AAs is not total. This should be attributed to the delicate but complex balance among interactions. More specifically, in a molecular distribution of AAs inside the fibers, the release would be exclusively affected by the balance between AA⋯polymer and AA⋯solvent interactions, the former and the latter being against and in favor, respectively, of the release. However, in this case AAs are not distributed at the molecular level (*i.e.* as individual molecules) but as crystals, as proved by both phase AFM images and XRD. Accordingly, AA⋯AA interactions, which in turn are affected by the geometry of the crystal, play a crucial role in the release process. It is worth noting that in many cases the latter interactions are expected to be strong because of their polar/charged nature. In addition, the strength of AA⋯solvent interactions in PE44/AA systems with AA crystals embedded inside polymeric matrix are expected to be restricted by the penetrability of the solvent into the fibers. Such two factors affect negatively to the release and explain the uncomplete release after 168 h. However, it should be emphasized that, in all cases, it was checked

that the sum of AA released along 168 h and the AA remaining at the PE44 matrix corresponded to the amount of AA loaded during the electrospinning process (see Methods).

*Release in enzymatic medium*. Profiles obtained using a lipase-containing medium evidences a very fast AA release (Figure 8d). The amount of AA retained after only 1 h is lower than 30% in all cases with the exception of Phe and Asp, which display values not very far from that value (47% and 35%, respectively). This should be attributed to a burst effect that is probably more pronounced for PE44/AA systems with AA crystal near the surface. Thus, in such systems the specific surface that is contact with the enzymatic medium is high, favoring the instability of AA particles. All the AAs reach the maximum release is reached after only 6 h, and it remains stable for the following 18 h. Furthermore, it is worth noting that the amount of AA retained in the fibre mats after 24 h is very small (Figure 8b), ranging from 5 % (Ala) to 27% (Phe). This represents a very remarkable difference with respect to the AA release in PBS and, especially, PBS-EtOH (Figure 8b).

In summary, results from release experiments in PBS, PBS-EtOH and the enzymatic solution prove that PE44 fibers are a very promising vehicle to supply AAs. Thus, the AAs are retained at the polymeric matrix not only in PBS but also in PBS-EtOH, which is a powerful extraction medium. In contrast, lipase, which is a key enzyme in the digestion process, favors a fast release. Overall, these results are consistent with the use of electronspun fibers as carriers for the contribution of AAs to the feed.

**Hydrolytic, enzymatic and accelerated degradation of loaded nanofibers**

In order to prove that PE44/AA NFs resist hydrolysis, accelerated degradation assays were performed by incubating unloaded PE44 and PE44/AA-10 mats in an aggressive 1

N NaOH solution for 30 min. It is worth noting that accelerated assays in acidic conditions are not required since the pH in the digestive system is < 7 and, therefore, preservation of the loading under such conditions is not required. In opposition, the delivery of loaded AAs should be prevented in basic conditions, which could be accidentally reached by food-containing PE44/AA fibers (*e.g.* during the storage). Representative SEM micrographs of the NFs after such incubation time are displayed in Figure 9. Unloaded PE44 NFs underwent a very fast hydrolytic degradation that produced erosion phenomena at their surface. This feature is corroborated in Figure S5, which shows a SEM micrograph of unloaded NFs after 3 h in the same basic solution. In opposition, PE44/AA-10 fibers remained unaltered in the NaOH solution. This feature has been attributed to the buffering capacity of the positively charged N-terminal group of the AA, which protects the polymeric matrix from the attack of hydroxyl groups. Similar buffering activity has been previously observed in other materials with charged groups.[42] The overall of these results is fully consistent with the AAs retention determined from release assays in PBS and PBS-EtOH.

On the other hand, the enzymatic degradation of the PE44/AA-10 mats was performed by incubating the samples in a lipase-containing medium. Analysis of the resulting profiles, which are displayed in Figure 10a, reflects a relatively fast degradation stage after the first two days: the weight loss (Eq. 1) ranges from 7% (PE44/Cys-10) to 16% (PE44/Lys-10) after such short period. However, the weight loss increases by less than 3% during the following 26 days evidencing that, after the initial degradation stage, the enzymatic degradation of PE44 NFs is very slow (*i.e.* the weight loss after 28 days ranges from 9% to 19% only). SEM micrographs displayed in Figure 10b correspond to PE44/AA-10 NFs after 2 days of incubation in the lipase-containing solution. Although erosion is not evident in many cases (*e.g.* Phe and Cys loaded NFs),

some morphological changes are detected at the surface of PE44/Lys-10, which experienced the highest weight loss. Hence, the enzymatic release of AAs from PE44 loaded NFs cannot be attributed to a fast and unspecific lipase-induced decomposition of the polymeric matrix. On the contrary, the enzymatic attack preferentially affected the ester bonds that keep the AA domains into the biphasic system, thus promoting their release. Probably, the morphological defects at the boundary limits between phases induced this specificity due to the higher accessibility of the enzyme into the polymeric fragments that retain the AA domains. This hypothesis is consistent with the fact that the highest weight loss in the enzymatic degradation assays corresponds to NFs loaded with charged AAs (*i.e.* SEM micrographs and AFM images revealed that Lys and Asp domains are preferentially embedded at the surface of NFs).

## CONCLUSIONS

In the light of the difficulties associated with AAs retention in delivery vehicles exposed to humid environments and their effective release after ingestion, we propose the loading of AAs into PE44 NFs using an electrospinning process as a reliable approach. Electrospun PE44/AA NFs can be described as biphasic systems made of AA crystals distributed into a polymeric matrix. The chemical nature of the AA has a deep impact on the distribution of such crystals, affecting also the properties of electrospun NFs. PE44 NFs have been proved to be very stable systems, able to retain loaded non-polar, polar and charged AAs in aqueous environments of different polarities and to deliver them very rapidly in enzymatic media. The physical characteristics of loaded PE44/AA NFs as well as their behaviour to effectively supply essential and conditional AAs suggest that they can be incorporated into the diets of livestock and fish in farms for administration.

It should be noted that electrospun fibres of biodegradable polymers loaded with biomolecules (*e.g.* growth factor, biocides, antibiotics and anticoagulants) are typically used in the biomedical field as scaffolds for cell regeneration. However, our approach can be used in the agro-food biotechnology field, solving an important problem like is the contribution of essential and conditional AAs to the feed. Obviously, the use of this strategy is not restricted to PE44 but it can be extended to other biodegradable polymers and biopolymers, such as for example poly(lactic acid) and poli(γ-glutamic acid). We are currently investigating the influence of this extrapolation on the release of loaded AAs.

## ACKNOWLEDGEMENTS

Authors acknowledge MINECO / FEDER (MAT2015-69367-R, MAT2015-69547-R and CTQ2013-40855-R) and Gobierno de Aragón–Fondo Social Europeo (research group E40) for financial support. C.A. is grateful to "ICREA Academia" program for support to the research.

## REFERENCES

1. A. B. Hughes, Amino Acids, Peptides and Proteins in Organic Chemistry, Vol 1-5, Wiley-VCH, Weinheim, 2009-2013.

2. O. W. Griffith, *Free Radic. Biol. Med.* **1999**, *27*, 922–935.

3. S. C. Lu, *B.B.A.-Gen. Subjects* **2013**, *1830*, 3143–3153.

4. M. C. Nlend, D. M. Cauvi, N. Venot, O. Chabaud, *Endrocrinol.* **2005**, *146*, 4834–4843.

5. S. M. Morris, *J. Nutr.* **2007**, *137*, 1602S–1609S.

6. S. Nagase, K. Takemura, A. Ueda, A. Hirayama, K. Aoyagi, M. Kondoh, A. Koyama, *Biochem. Biophys. Res. Commun.* **1997**, *233*, 150–153.

7. N. W. Rajapakse, D. L. Mattson, *Curr. Opin. Nephrol. Hypertens.* **2013**, *22*, 45–50.

8. J. Yan, G. Tie, L. M. Messina, *Mol. Med.* **2012**, *18*, 1220–1230.

9. B. Hernández-Ledesma, M. M. Contreras, I. Recio, *Adv. Colloid Interface Sci.* **2001**, *165*, 23–35.

10. J. Renukuntla, A. D. Vadlapudi, A. Patel, S. H. S. Boddu, A. K. Mitra, *Int. J. Pharm.* **2013**, *447*, 75–93.

11. X. Gao, C. He, C. Xiao, X. Zhuang, X. Chen, *Polymer* **2013**, *54*, 1786–1793.

12. C. Dai, B. Wang, H. Zhao, *Colloids Surf. B Biointerfaces* **2005**, *41*, 117–120.

13. D. Hennig, S. Schubert, H. Dargatz, E. Kostenis, A. Fahr, U. S. Schubert, T. Heinzel, D. Imhof, *Macromol. Biosci.* **2014**, *14*, 69–80.

14. L. Li, Q. Wang, H. Li, M. Yuan, M. Yuan, *PLOS one* **2014**, *9*, e100809.

15. G. Fabregat, B. Teixeira-Dias, L. J. del Valle, E. Armelin, F. Estrany, C. Alemán, *ACS Appl. Mater. Interfaces* **2014**, *6*, 11940–11954.

16. C. J. Langdon, *Aquaculture* **2003**, *227*, 259–275.

17. J. López-Alvarado, C. J. Langdon, S. I. Teshima, A. Kanazawa, *Aquaculture* **1994**, *122*, 335–346.

18. S. K. Tonheim, W. Koven, I. Rønnestad, *Aquaculture* **2000**, *190*, 223–235.

19. C. Langdon, B. Clack, U. Önal, *Aquaculture* **2007**, *268*, 143–148.

20. S. Z. Mohammady, M. Pouzot, R. Mezzenga, *Biophys. J.* **2009**, *96*, 1537–1546.

21. C. J. Sánchez Jr., E. M. Prieto, C. A. Krueger, K. J. Zienkiewicz, D. R. Romano, C. I. Ward, K. S. Akers, S. A. Guelcher, J. C. Wenke, *Biomaterials* **2013**, *34*,7533-7543.

22. S. Maione, L. J. del Valle, M. M. Pérez-Madrigal, C. Cativiela, J. Puiggalí, C. Alemán, *RSC Adv.* **2016**, *6*, 73045–73055.

23. M. M. Pérez, E. Llorens, L. J. del Valle, J. Puiggalí, E. Armelin, C. Alemán, *Express Polym. Lett.* **2016**, *10*, 628–646.

24. I. Sebe, P. Szabó, B. Kállai-Szabó, R. Zelko, *Int. J. Pharm.* **2015**, *494*, 516–530.

25. A. Díaz, R. Katsarava, J. Puiggalí, *Int. J. Mol. Sci.* **2014**, *15*, 7064–7123.

26. E. Armelin, A. L. Gomes, M. M. Pérez-Madrigal, J. Puiggalí, L. Franco, L. J. del Valle, A. Rodríguez-Galán, J. S. de C. Campos, N Ferrer-Anglada, C. Alemán, *J. Mat. Chem.* **2012**, *22*, 585–594.

27. E. Llorens, E. Armelin, M. M. Pérez-Madrigal, L. J. del Valle, C. Alemán, J. Puiggalí, *Polymers* **2013**, *5*, 1115–1157.

28. K. Ghosal, A. Manakhov, L. Zajickova, S. Thomas, *AAPS Pharm. Sci. Tech.* **2016**, in press. doi:10.1208/s12249-016-0500-8.

29. D. Li, Y. Xia, *Adv. Mater.* **2004**, *16*, 1151–1170.

30. L. J. del Valle, R. Camps, A. Díaz, L. Franco, A. Rodríguez-Galán, J. Puiggalí, *J. Polym. Res.* **2011**, *18*, 1903–1917.

31. S. L. Shenoy, W. D. Bates, H. L. Frisch, G. E. Wnek, *Polymer* **2005**, *46*, 3372-3384.

32. E. S. Yoo, S. S. Im, *J. Polym. Sci. Polym. Phys.* **1999**, *37*, 1357–1366.

33. V. M. Correlo, L. F. Boesel, E. Pinho, A. R. Costa-Pinto, M. L. Alves da Silva, M. Bhattacharya, J. F. Mano, N. M. Neves, R. L. Reis, *J. Biomed. Mater. Res.* **2009**, *91A*, 489–504.

34. Z. Qiu, W. Yang, *Polymer* **2006**, *47*, 6429–6437.

35. L. Song, Z. Qiu, *Polym. Degrad. Stab.* **2009**, *94*, 632−637.

36. J. Hay, J. Langford, J. Lloyd, *Polymer* **1989**, *30*, 489−493.

37. H. Klug, L. Alexander, X-Ray Diffraction Procedure for Polycrystallite and Amorphous Materials, 2nd. Edition, John Wiley and Sons, New York, 1974.

38. E. H. Jeong, S. S. Im, J. H. Youk, *Polymer* **2005**, *46*, 9538−9543.

39. V. Tserki, P. Matzinos, E. Pavlidou, D. Vachliotis, C. Panayiotou, *Polym. Degrad. Stab.* **2006**, *91*, 367−376.

40. X .Zong, K. Kim, D. Fang, S. Ran, B. S. Hsiao, B. Chu, *Polymer* **2002**, *43* 4403−4412.

41. R. Baker, Controlled release of biologically active agents, Wiley & Sons, Eds.; New York, Chapter 4, 1987.

42. L. J. del Valle, O. Bertran, G. Chaves, G. Revilla-López, M. Rivas, M. T. Casas, J. Casanovas, P. Turon, J. Puiggalí, C. Alemán, *J. Mater. Chem. B* **2014**, *2*, 6953–6966.

## CAPTIONS TO FIGURES

**Figure 1.** FTIR spectra of electrospun PE44, PE44/Phe-10, PE44/Asn-10 and PE44/Lys-10 fibres in the range 1800-1450 $cm^{-1}$. Absorption bands marked with boxes have been used to identify the AA in the loaded fibres (see text).

**Figure 2.** Representative SEM micrographs of PE44, PE44/Ala, PE44/Phe, PE44/Cys, PE44/Asn, PE44/Lys and PE44/Asp electrospun fibres.

**Figure 3.** AFM images of (a) PE44/Ala-1, (b) PE44/Asn-1 and (c) PE44/Lys-1: 2D topography (left) and phase (right) images. The scan window sizes were $2\times2$ $\mu m^2$, whereas zoomed areas correspond to $250\times250$ $nm^2$ windows.

**Figure 4.** AFM images of (a) PE44/Ala-10 and (b) PE44/Asn-10: 2D topography (left) and phase (right) images. The scan window sizes were $500\times500$ $nm^2$.

**Figure 5.** TGA and DTGA curves (shown in inset) of all studied samples.

**Figure 6.** DSC curves indicating the first heating run (a), the cooling run (b) and the third heating run (c) of PE44 ( dashed black line) , Pe44/Phe-10 (solid red line) and Pe44/Asn-10 (solid blue line). Inset shows endothermic peaks associated to AAs degradation process.

**Figure 7.** WAXD patterns of unloaded and loaded fibres matrices: (a) unloaded PE44; (b) PE44/Ala-10; (c) PE44/Phe-10; (d) PE44/Cys-10; (e) PE44/Asn-10; (f) PE44/Lys-10 and (g) PE44/Asp-10. Circles correspond to the observed XRD profiles while red lines are calculated profiles. Insets in (b)-(g) correspond to the XRD profiles of crystallized AAs. The deconvolution of the XRD profile (right) is also displayed for unloaded PE44 (a).

**Figure 8.** Accumulated release profiles of AAs from PE44/AA-10 NFs in (a) PBS, (c) PBS-EtOH and (d) a lipase-containing medium. The amount of AA retained after 168 h (PBS and PBS-EtOH) or 24 h (lipase-containing medium) is represented in (b).

**Figure 9.** SEM micrographs of PE44/Phe-100, PE44/Asn-10, PE44/Asp-10 and unloaded PE44 after 30 min of immersion in 1 N NaOH.

**Figure 10.** (a) Weight loss profiles of PE44/AA-10 NFs in 1 N NaOH solution. (b) SEM micrographs of PE44/AA-10 after 2 days of incubation in the lipase-containing solution.

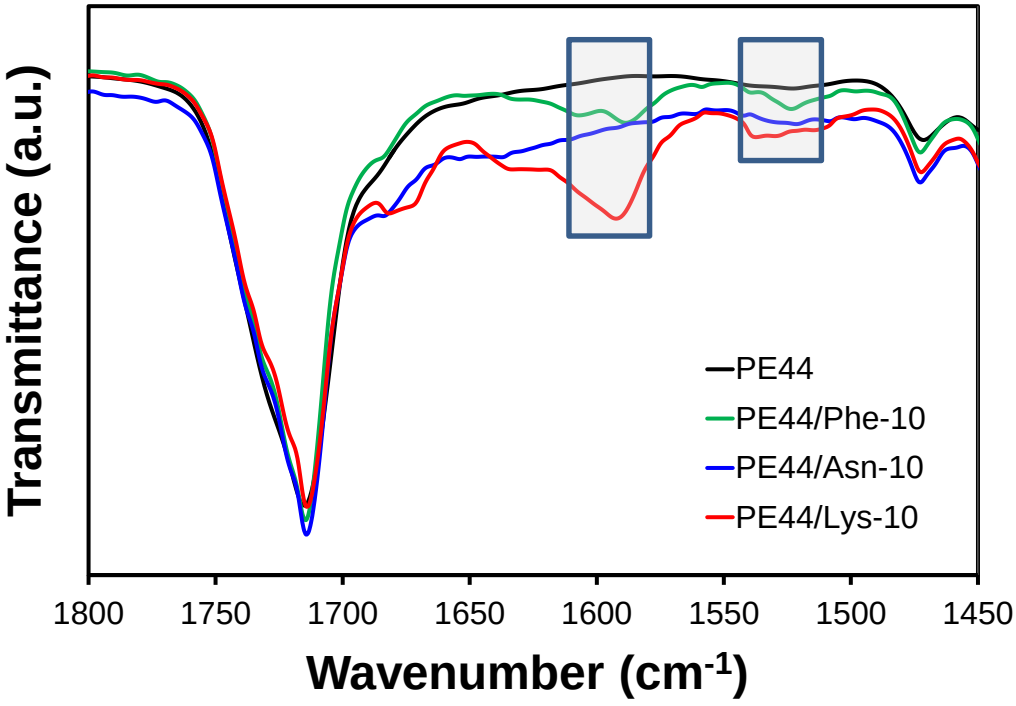
Transmittance (a.u.)
1800
1750
1700
1650
1600
1550
1500
1450
Wavenumber (cm-1)
PE44
PE44/Phe-10
PE44/Asn-10
PE44/Lys-10

Figure 1

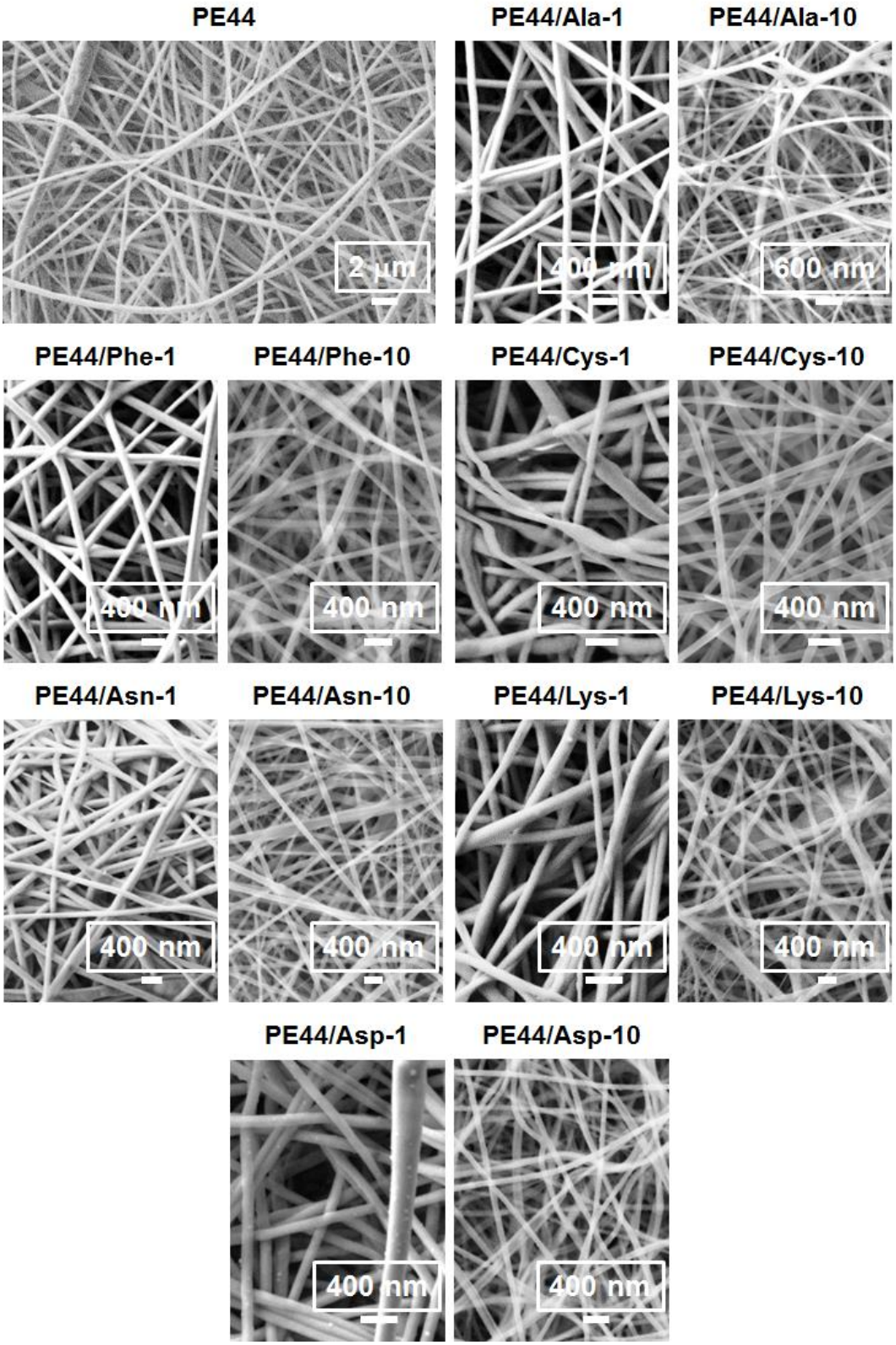
PE44
PE44/Ala-1
PE44/Ala-10
2 μm
400 nm
600 nm
PE44/Phe-1
PE44/Phe-10
PE44/Cys-1
PE44/Cys-10
400 nm
400 nm
400 nm
400 nm
PE44/Asn-1
PE44/Asn-10
PE44/Lys-1
PE44/Lys-10
400 nm
400 nm
400 nm
400 nm
PE44/Asp-1
PE44/Asp-10
400 nm
400 nm

Figure 2

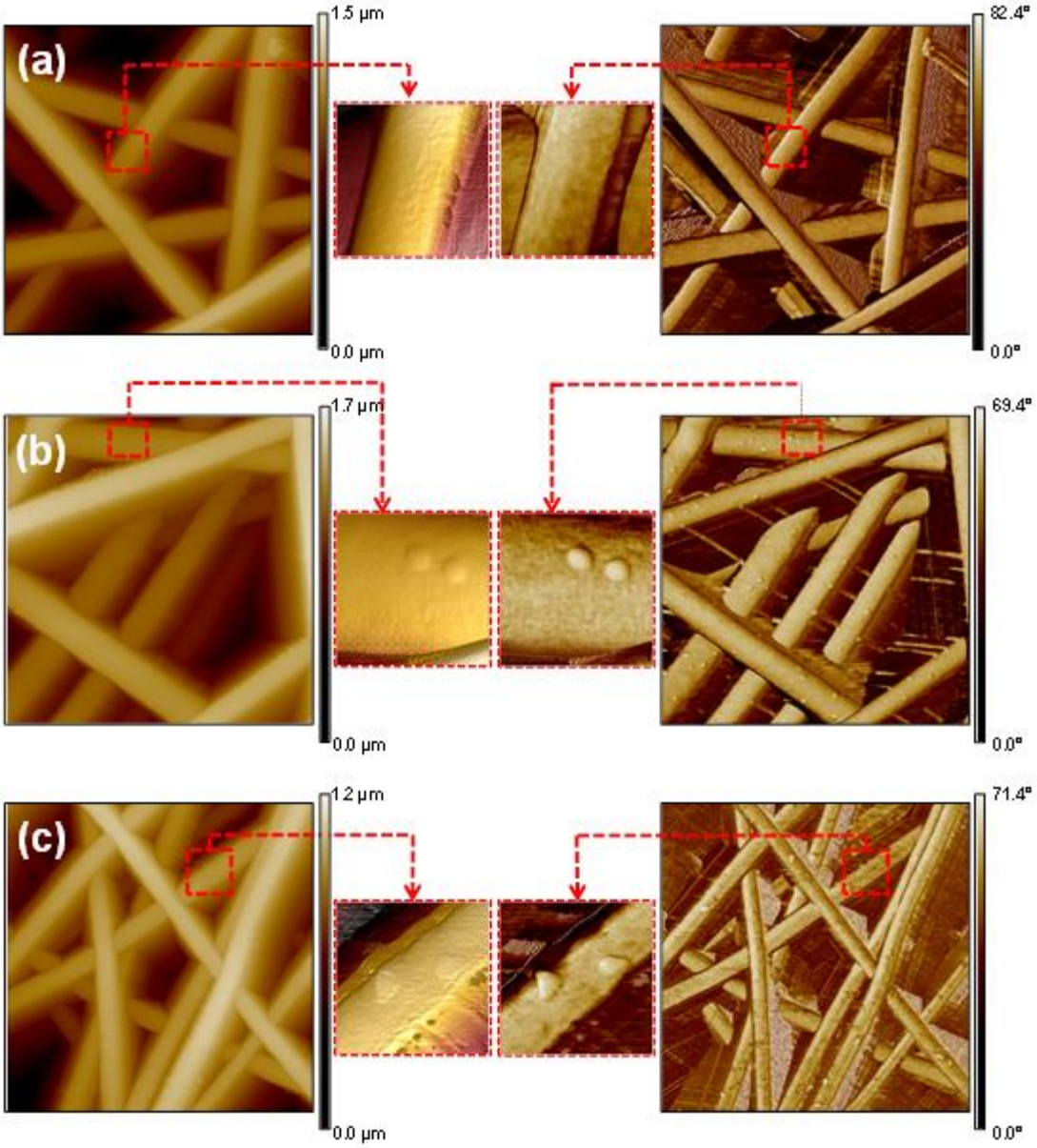


Figure 3

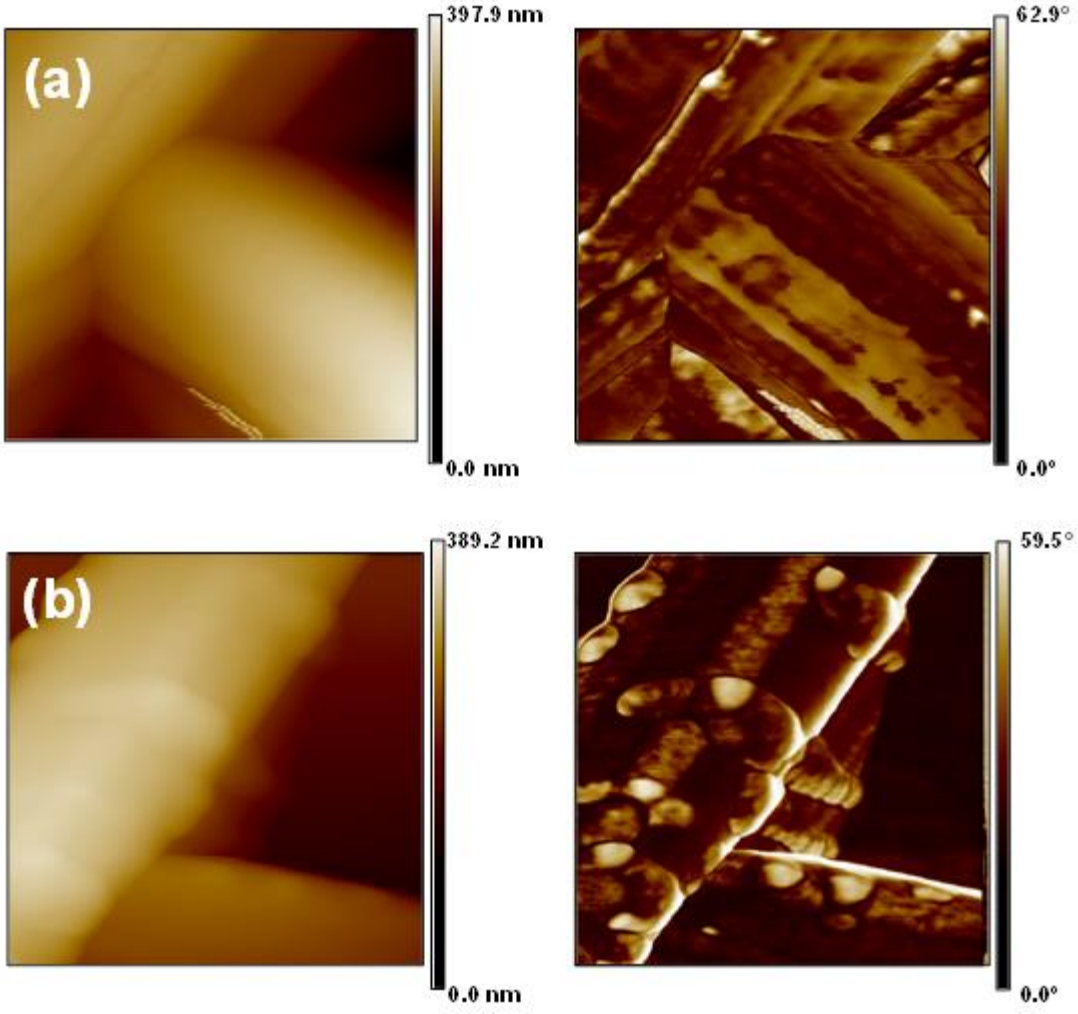


Figure 4

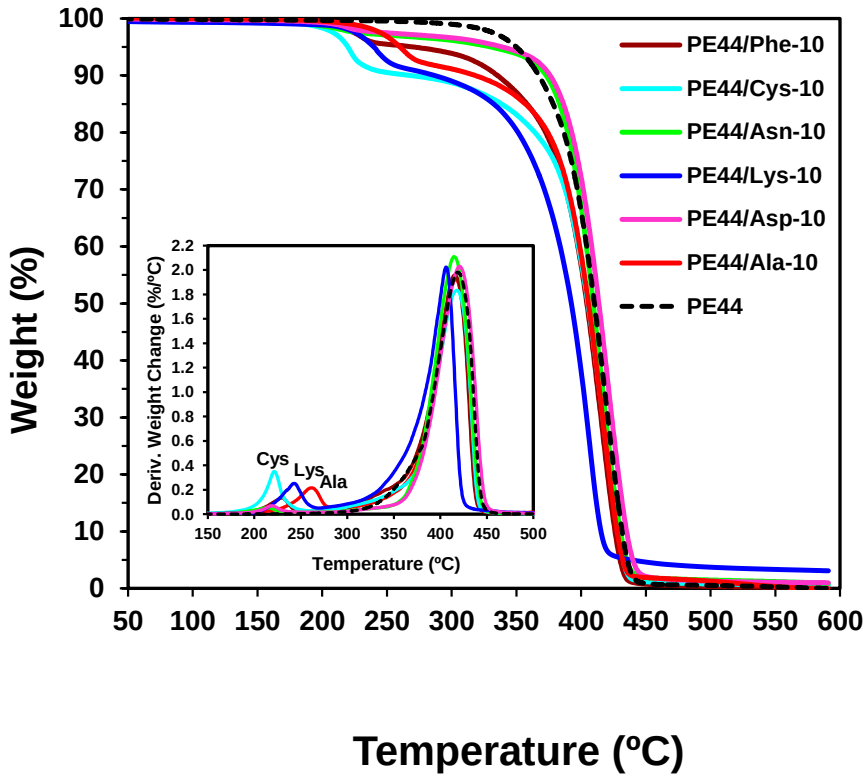
Weight (%)
Temperature (ºC)
PE44/Phe-10
PE44/Cys-10
PE44/Asn-10
PE44/Lys-10
PE44/Asp-10
PE44/Ala-10
PE44
Deriv. Weight Change (%/ºC)
Cys
Lys
Ala
Temperature (ºC)

Figure 5

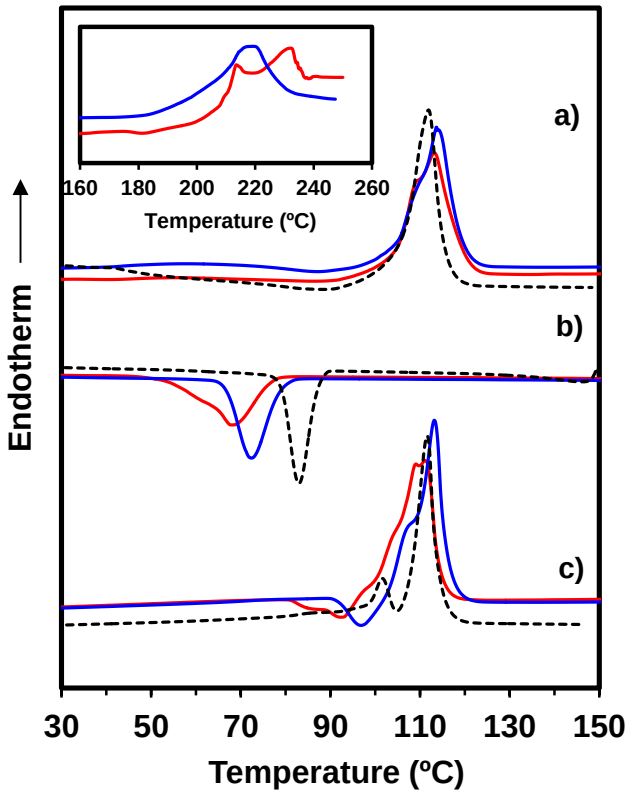
a)
b)
c)
160
180
200
220
240
260
Temperature (ºC)
Endotherm
30
50
70
90
110
130
150
Temperature (ºC)

Figure 6

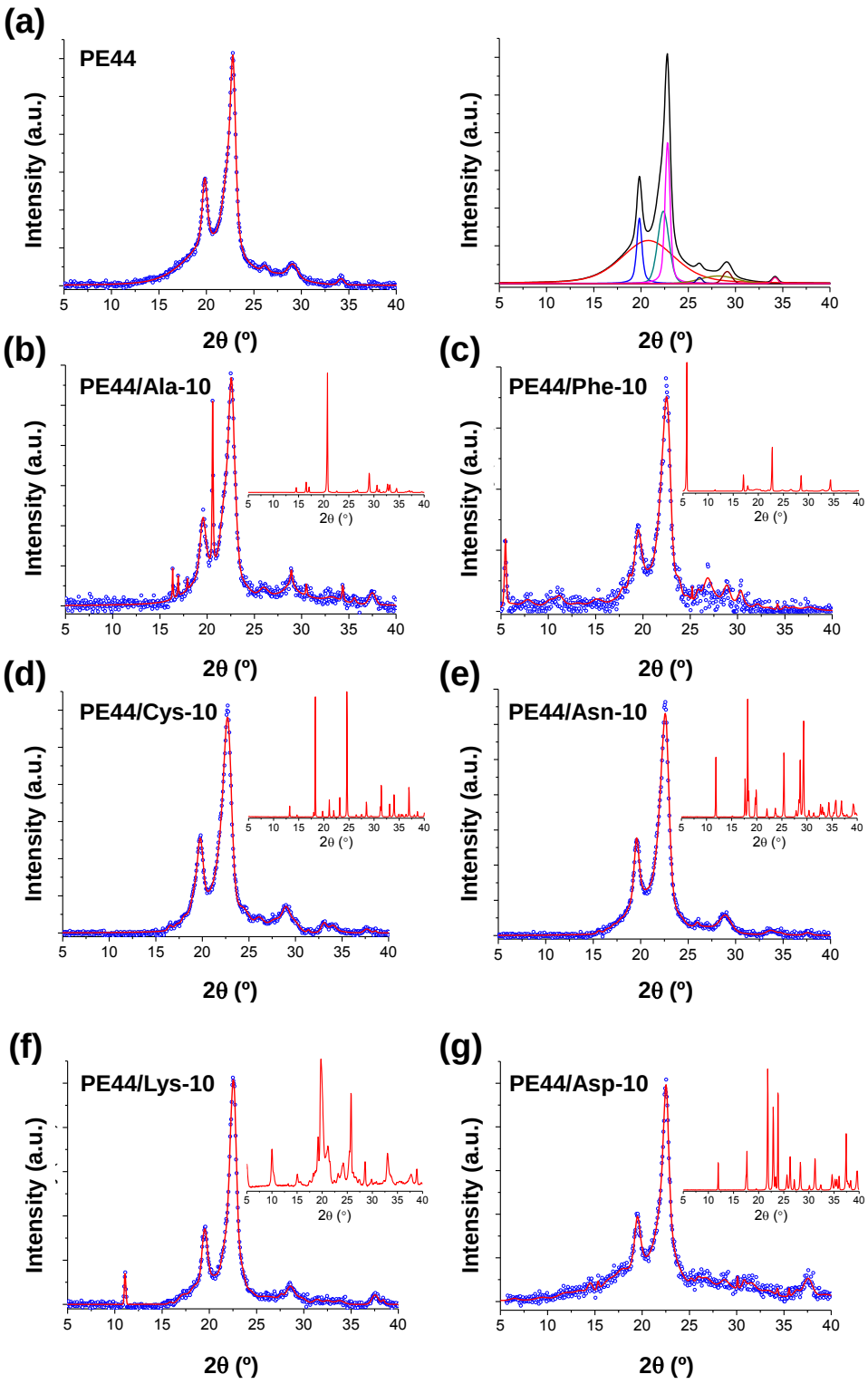
(a)
PE44
Intensity (a.u.)
2θ (°)
(b)
PE44/Ala-10
(c)
PE44/Phe-10
(d)
PE44/Cys-10
(e)
PE44/Asn-10
(f)
PE44/Lys-10
(g)
PE44/Asp-10

Figure 7

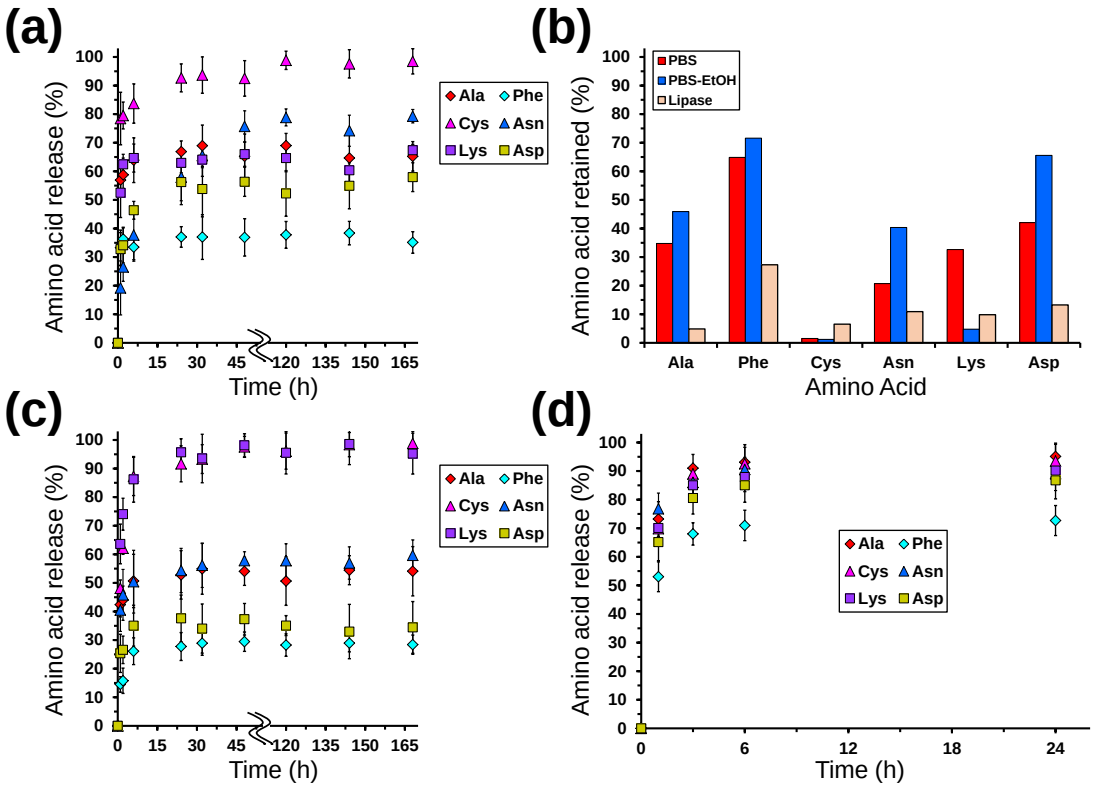
(a)
Amino acid release (%)
Time (h)
Ala
Phe
Cys
Asn
Lys
Asp
(b)
Amino acid retained (%)
PBS
PBS-EtOH
Lipase
Amino Acid
(c)
Amino acid release (%)
Time (h)
(d)
Amino acid release (%)
Time (h)

Figure 8

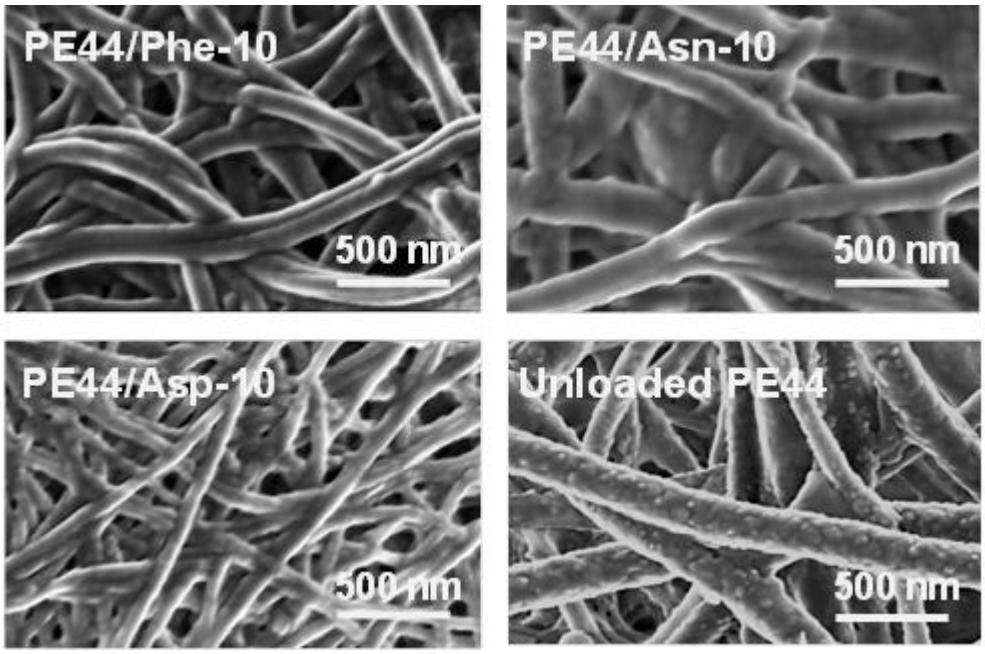
PE44/Phe-10
500 nm
PE44/Asn-10
500 nm
PE44/Asp-10
500 nm
Unloaded PE44
500 nm

Figure 9

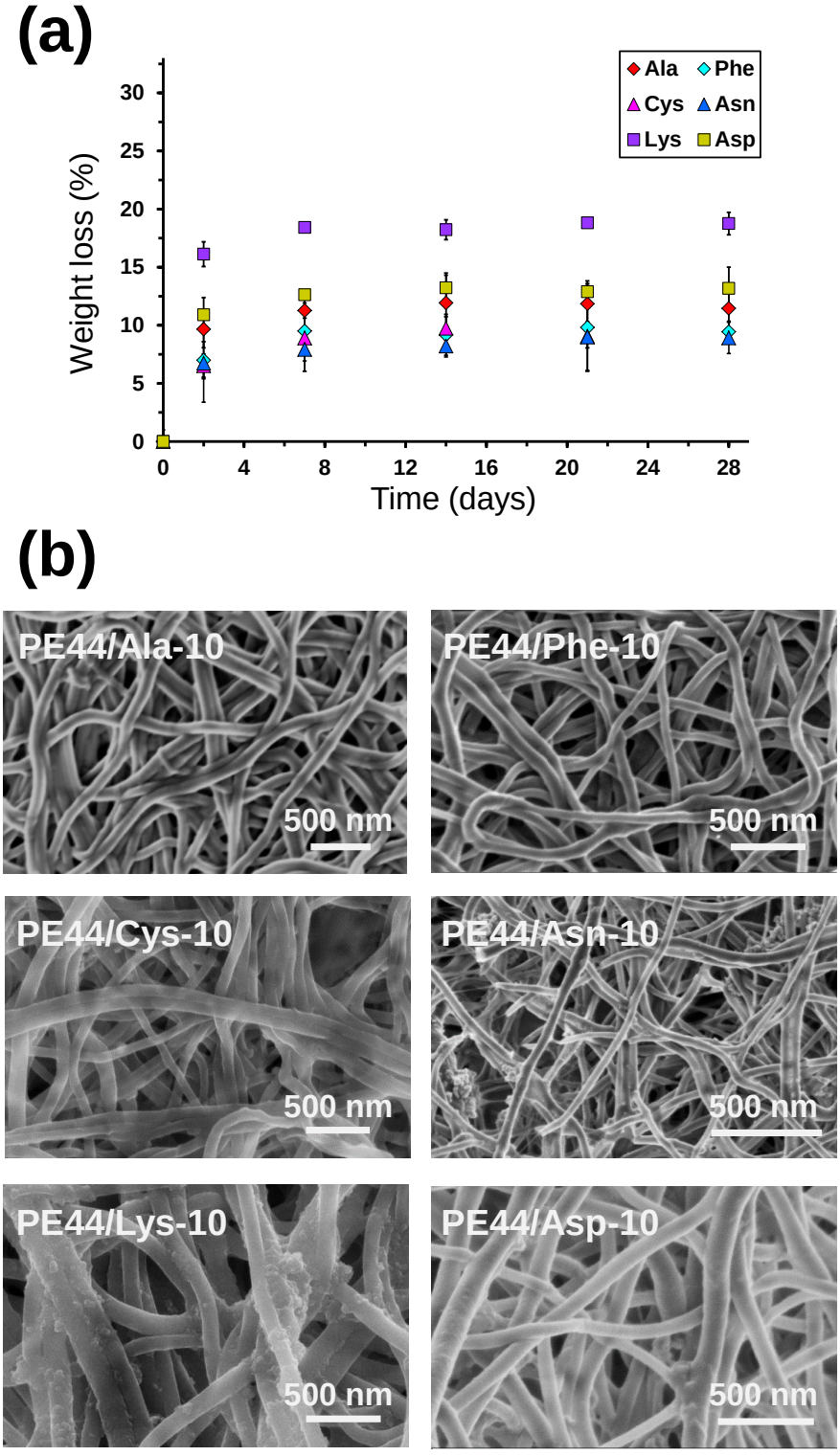
(a)
Ala
Phe
Cys
Asn
Lys
Asp
Weight loss (%)
0
5
10
15
20
25
30
0
4
8
12
16
20
24
28
Time (days)
(b)
PE44/Ala-10
500 nm
PE44/Phe-10
500 nm
PE44/Cys-10
500 nm
PE44/Asn-10
500 nm
PE44/Lys-10
500 nm
PE44/Asp-10
500 nm

Figure 10

**Table 1.** Average diameter and standard deviation ($D_{av}$ ± σ) of electrospun fibres prepared in this work.

| System | $D_{av}$ (nm) ± σ (nm) | System | $D_{av}$ (nm) ± σ (nm) |
|---|---|---|---|
| PE44 | 386 ± 121 | - | |
| PE44/Ala-1 | 120 ± 24 | PE44/Ala-10 | 108 ± 30 |
| PE44/Phe-1 | 140 ± 31 | PE44/Phe-10 | 91 ± 16 |
| PE44/Cys-1 | 109 ± 28 | PE44/Cys-10 | 91 ± 13 |
| PE44/Asn-1 | 119 ± 26 | PE44/Asn-10 | 116 ± 29 |
| PE44/Lys-1 | 99 ± 19 | PE44/Lys-10 | 130 ± 37 |
| PE44/Asp-1 | 108 ± 20 | PE44/Asp-10 | 83 ± 16 |

**Table 2.** Root mean square roughness and standard deviation ($D_{av} \pm \sigma$) values for the fibre surface of the electrospun samples displayed in Figure 2 and 3.

| System | Rq (nm) ± σ (nm) | System | $D_{av}$ (nm) ± σ (nm) |
|---|---|---|---|
| PE44 | 3.2 ± 1.1 | - | |
| PE44/Ala-1 | 6.4 ± 1.7 | PE44/Lys-1 | 10.2 ± 2.4 |
| PE44/Phe-1 | 5.3 ± 1.1 | PE44/Asp-1 | 9.5 ± 2.4 |
| PE44/Cys-1 | 8.5 ± 2.8 | PE44/Phe-10 | 4.3 ± 1.2 |
| PE44/Asn-1 | 7.7 ± 1.7 | PE44/Asn-10 | 6.3 ± 1.8 |

**Table 3.** Thermogravimetric data of PE44 and PE44/AAs samples.

| Sample | $T_{1\%}$ (ºC) [a] | $T_{3\%}$ (ºC) [a] | $T_{max}$ (ºC) [b] | $T_{max}$ (ºC) [b] | $\%W_{(500ºC)}$ [a] |
|---|---|---|---|---|---|
| PE44 | 299 | 337 | - | 419 | 0.52 |
| PE44/Ala-10 | 222 | 249 | 261 | 417 | 1.27 |
| PE44/Phe-10 | 203 | 228 | 229 | 415 | 0.33 |
| PE44/Cys-10 | 185 | 212 | 221 | 417 | 0.77 |
| PE44/Asn-10 | 189 | 256 | 213 | 414 | 1.47 |
| PE44/Lys-10 | 184 | 229 | 243 | 405 | 3.72 |
| PE44/Asp-10 | 209 | 280 | 218 | 421 | 1.27 |

[a] Determined from the TGA curve
[b] Determined from the DTGA curve

**Table 4.** Calorimetric data of the PE44, PE44/Asn-10 and PE44/Phe-10 samples

| Sample | 1st Heating run | | Cooling run | | 2nd Heating run | |
|---|---|---|---|---|---|---|
| | $T_m$ (°C) | $\Delta H_m$ (J/g) | $T_c$ (°C) | $\Delta H_c$ (J/g) | $T_m$ (°C) | $\Delta H_m$ (J/g) |
| PE44 | 111.9 | 70.8 | 82.0 | 72.0 | 101.6, 111.6 | 74.0 |
| PE44/Asn-10 | 113.7, 108.6[a] | 71.1 | 72.4 | 67.3 | 113.2 | 70.9 |
| PE44/Phe-10 | 113.2, 108.8[a] | 68.8 | 68.0 | 67.5 | 111.1 | 72.4 |

[a] Small shoulder

**Table 5.** Crystallinity degree ($\chi_c$; Eqn 1) and crystallite size in the direction perpendicular to the representative (*hkl*) planes ($L_{(hkl)}$; Eqn 2) for unloaded PE44 and PE44/AA-10 fibres.

| | $\chi_c$ | $L_{(020)}$ (nm) | $L_{(021)}$ (nm) | $L_{(110)}$ (nm) |
|---|---|---|---|---|
| PE44 | 0.47 | 11.67 | 5.29 | 11.59 |
| PE44/Ala-10 | 0.55 | 10.49 | 7.18 | 9.94 |
| PE44/Phe-10 | 0.66 | 9.31 | 5.87 | 8.70 |
| PE44/Cys-10 | 0.67 | 10.75 | 4.93 | 8.02 |
| PE44/Asn-10 | 0.74 | 11.54 | 5.91 | 8.47 |
| PE44/Lys-10 | 0.72 | 11.10 | 9.26 | 10.50 |
| PE44/Asp-10 | 0.58 | 9.68 | 4.55 | 10.62 |